The Effect of the Combustor-Turbine Slot and Midpassage Gap on Vane Endwall Heat Transfer

Stephen P. Lynch

Karen A. Thole

Department of Mechanical and Nuclear Engineering,
The Pennsylvania State University,
University Park, PA 16802

Turbine vanes are generally manufactured as single- or double-airfoil sections that are assembled into a full turbine disk. The gaps between the individual sections, as well as a gap between the turbine disk and the combustor upstream, provide leakage paths for relatively higher-pressure coolant flows. This leakage is intended to prevent ingestion of the hot combustion flow in the primary gas path. At the vane endwall, this leakage flow can interfere with the complex vortical flow present there and thus affect the heat transfer to that surface. To determine the effect of leakage flow through the gaps, heat transfer coefficients were measured along a first-stage vane endwall and inside the midpassage gap for a large-scale cascade with a simulated combustor-turbine interface slot and a midpassage gap. For increasing combustor-turbine leakage flows, endwall surface heat transfer coefficients showed a slight increase in heat transfer. The presence of the midpassage gap, however, resulted in high heat transfer near the passage throat where flow is ejected from that gap. Computational simulations indicated that a small vortex created at the gap flow ejection location contributed to the high heat transfer. The measured differences in heat transfer for the various midpassage gap flowrates tested did not appear to have a significant effect. [DOI: 10.1115/1.4002950]

1 Introduction

The need to further improve turbine engine efficiencies drives engine designs toward higher turbine inlet temperatures and lower required coolant for hot gas path hardware. Turbine hardware downstream of the combustor is subjected to combustion gas temperatures in excess of the metal melting temperature, and cooling is required to maintain part durability. The coolant, generally extracted from the compressor, results in an efficiency penalty since it provides no useful work in the turbine, and thus it is desirable to minimize the amount needed.

In an engine, high-pressure coolant is designed to leak through gaps between individual components that comprise the turbine section to prevent hot gas ingestion. The nozzle guide vane section downstream of the combustor is generally composed of single- or double-airfoil sections assembled into a ring. A gap is present between each airfoil section in the ring, which will be referred to as a midpassage gap in this paper. Furthermore, the turbine vane ring is physically separated from the combustor, resulting in a slot at the interface between the two, which will be referred to as an upstream slot in this paper. This gap and slot between components are a necessary consequence of the manufacturing and assembly process, but also help to accommodate thermal expansion over the wide range of turbine operating conditions.

As previously mentioned, coolant is designed to leak through these leakage paths to prevent hot gas ingestion, but has the inherent advantage that the fluid can be used to provide cooling coverage for the component. Until fairly recently, however, these leakage paths were mostly neglected in studies of endwall heat transfer and turbine aerodynamic loss. Recent studies outlined in the literature review indicate that the presence of slots and gaps has significant effects on the endwall film-cooling effectiveness and heat transfer.

In this study, a realistic endwall slot and gap were studied in a scaled-up nozzle guide vane cascade. The combustor-turbine interface gap was modeled as a two-dimensional slot. The midpassage gap ran through the middle of the vane passage and divided it into pressure-side (PS) and suction-side (SS) platforms. The effect of the upstream slot and the midpassage gap on the endwall heat transfer will be discussed in this paper.

2 Relevant Past Studies

A range of studies have been presented in the literature concerning the effect of turbine component interface gaps on turbine aerodynamics and film-cooling. Leakage flows from slots between the combustor and turbine, as well as from mating gaps between individual vanes or blades, have been shown to have significant interactions with the mainstream flow and significant effects on endwall cooling. Few studies exist, however, for the associated endwall heat transfer. In this review, studies considering only the effect of the combustor-turbine interface are presented first, followed by studies considering the addition of a midpassage gap.

Effectiveness measurements and predictions were presented by Knost and Thole [1] for a vane endwall with cooling from an upstream slot. Coolant exited nonuniformly from the upstream slot and was swept to the suction side of the passage, leaving a large uncooled area near the vane pressure side when no discrete film-cooling holes were present in the passage. Using the same vane geometry, Lynch and Thole [2] measured a much more uniform slot injection by placing the same slot further upstream ($0.77C_{ax}$ upstream of the vane stagnation versus $0.3C_{ax}$ for Knost and Thole [1]). Flowfield and heat transfer measurements by Rehder and Dannhauer [3] indicated leakage exiting a slot with a backward-facing step in which the flow was directed tangentially, tended to re-energize the incoming boundary layer and reduce the development of the horseshoe vortex. Conversely, slot flow that was ejected normal to the hot gas flow direction strengthened the horseshoe vortex and increased losses.

The aerodynamic impact of leakage flow injected into the passage between airfoils was studied by Aunapu et al. [4], who applied blowing into the mainstream from wall jets to break up the passage vortex. While the jets prevented the passage vortex from impinging on the suction side of the passage, the jets did not

Contributed by the International Gas Turbine Institute (IGTI) of ASME for publication in the JOURNAL OF TURBOMACHINERY. Manuscript received May 19, 2010; final manuscript received June 4, 2010; published online April 19, 2011. Editor: David Wisler.

decrease its strength. Reid et al. [5] studied aerodynamic losses arising from the presence of a midpassage gap between vane sections and found a decrease in stage efficiency even without any net leakage flow through the gap. Predictions of efficiency and exit yaw angle with and without the gap agreed well with measurements. In another paper, Reid et al. [6] reported that by shifting the gap closer to the pressure side, an increase in turbine efficiency occurred relative to the nominal gap location.

Piggush and Simon [7–9] presented a series of studies for a nozzle guide vane with axisymmetric endwall contouring and realistic endwall gap leakage features. In general, axisymmetric endwall contouring results in weaker secondary flows than a cascade with a flat endwall, and thus less interaction of the gap leakage flow with the secondary flow would be expected. Piggush and Simon [7] found through testing numerous conditions that the leakage from the midpassage gap was the most significant parameter in increasing exit total pressure loss. Endwall heat transfer measurements presented by Piggush and Simon [8] indicated that the presence of the midpassage gap resulted in increased heat transfer at the forward part of the gap where it ingested flow and thinned the endwall boundary layer. High heat transfer was also seen at the aft section of the gap where it ejected flow, relative to an endwall without a gap.

Adiabatic effectiveness measurements were presented by Piggush and Simon [9] for the same geometry as in Ref. [7]. They found that increasing the slashface gap blowing only slightly increased the cooling effectiveness downstream of the gap ejection location when compared with the nominal case. The study of Ranson et al. [10] also examined the endwall cooling effectiveness of leakage flows through both an upstream slot and a midpassage (featherseal) gap. Endwall adiabatic effectiveness levels were increased with increasing upstream slot leakage, but unchanged for a range of featherseal gap flows. Computational predictions of endwall effectiveness were higher than measured values immediately downstream of the slot, but agreed more closely further into the passage.

Cardwell et al. [11,12] found that the midpassage gap between vanes significantly altered the endwall cooling effectiveness relative to an endwall without a gap due to coolant ingestion into the gap. They also found that increasing the midpassage gap leakage flowrate did not have a measurable influence on endwall cooling effectiveness. Using the same geometry, the computational study of Hada and Thole [13] indicated disruption of the passage vortex due to ingestion near the forward part of the gap. Ejection of gap flow near the aft part of the gap also disrupted the passage vortex, and the ejected coolant increased endwall cooling effectiveness downstream of the vane trailing edge relative to an endwall without a gap.

As described above, the studies of Cardwell et al. [11,12] and Hada and Thole [13] indicated a significant effect of the midpassage gap on the vane endwall cooling effectiveness. This paper expands on those studies by considering the endwall heat transfer with a midpassage gap. It is important to note, however, that the endwall in this study differs from the studies of Cardwell et al. [11,12] and Hada and Thole [13] in that the endwall is not rough and does not have discrete hole film-cooling. The unique feature of this study relative to previous studies is the inclusion of heat transfer measurements on the inner channel walls of the midpassage gap.

3 Experimental Methodology

Measurements of endwall heat transfer were obtained in a scaled-up first-stage vane test section installed in a low-speed wind tunnel. The tunnel is depicted in Fig. 1 and is described in further detail by Lynch and Thole [2]. Flow through the tunnel was powered by an axial fan. Downstream of the fan, the flow passed through a heat exchanger and then was split into a core flow section and two bypass flow sections. The flow through the core section was sent through several flow conditioning screens. A convergence section downstream of the screens (3.9C upstream of the vane) initiated a new boundary layer on the endwall. Downstream of the convergence, the flow area remained constant entering the test section.

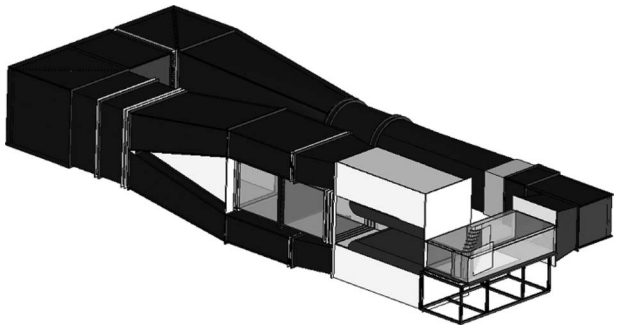

Fig. 1 Depiction of the large-scale wind tunnel with corner test section

The linear vane test section contained two full passages (see Fig. 2(*a*)), whereby the lower passage was bounded by a flexible wall to maintain the design pressure distribution along the center vane. The airfoils were based on the midspan geometry of a first-stage vane and scaled by a factor of 9 to allow for high measurement resolution. For this study, the vane Reynolds number was matched to engine conditions. Table 1 summarizes the geometry and flow conditions of the vane test section. See Kang et al. [14] and Radomsky and Thole [15] for more details about the cascade and its benchmarking.

The turbulent boundary layer approaching the test section was measured at a location 1.2C upstream of the vane. The boundary

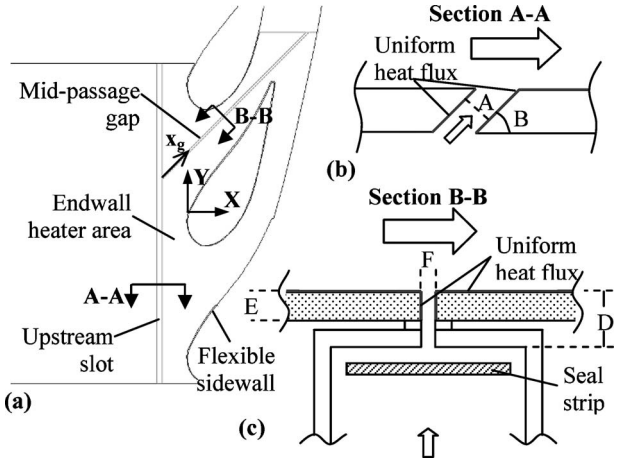

Fig. 2 (*a*) The vane test section with simulated upstream slot and midpassage gap leakage interfaces, (*b*) section view of upstream slot, and (*c*) section view of midpassage gap with seal strip; see Table 2 for dimensions

Table 1 Vane geometry and flow conditions

Scale factor	9
Scaled chord (C)	0.594 m
Axial chord/chord (C_{ax}/C)	0.49
Pitch/chord (P/C_{ax})	0.77
Span/chord (S/C_{ax})	0.93
Inlet Re ($\mathrm{Re}_{in}=CU_{in}/\nu$)	2.3×10^5
Exit Re ($\mathrm{Re}_{exit}=CU_{exit}/\nu$)	1.1×10^6
Inlet velocity (U_{in})	6.3 m/s
Inlet, exit flow angles	0 deg, 78 deg
Inlet, exit Mach	0.018, 0.090

Table 2 Leakage interface geometry

A	Upstream slot width	$0.024C$
	Slot flow length	$1.88A$
B	Injection angle	45 deg
	Distance upstream of vane	$-0.3C_{ax}$
D	Midpassage gap depth	$0.096C$
E	Heated gap depth	$0.44D$
F	Midpassage gap width	$0.011C$

Table 3 Slot and gap coolant settings

	MFR (%)	M	I
Slot	0.75	0.28	0.08
	0.85	0.32	0.11
	1.0	0.39	0.15
Gap	0	0	0
	0.3	0.17	0.03
	0.5	0.29	0.08

layer thickness at that location was $\delta/S=0.05$, the freestream turbulence level was 1%, and the momentum thickness Reynolds number was $\mathrm{Re}_\theta=1100$.

3.1 Leakage Interface Geometries. As described by Cardwell et al. [11,12], the flat endwall of the linear vane test section contained realistic leakage features including an interface slot between the combustor and the turbine and a midpassage gap between vane platforms. The endwall was cut from 2.54 cm thick polyurethane closed-cell foam for low conductivity losses during the heat transfer tests. A two-dimensional slot representing the interface between the combustor and the turbine was placed $0.3C_{ax}$ upstream of the vane, as shown in Fig. 2(*a*). This leakage interface will be referred to as the upstream slot. A section view of the slot is depicted in Fig. 2(*b*) with dimensions given in Table 2. For this study, strips of Inconel foil were attached to the inner channel walls of the upstream slot. Copper bus bars were soldered to the ends of the Inconel strips and connected to a power supply so that a uniform heat flux could be applied to the upstream slot faces.

The other realistic vane feature modeled for this study was a gap in the passage between the vanes, depicted in Fig. 2(*a*). This gap represents the interface between the vane sections that comprise a turbine disk and will be referred to as a midpassage gap. A detailed description of the midpassage gap design is given by Cardwell et al. [11,12], but a brief overview is also presented here. The centerline of the midpassage gap was angled at 45 deg relative to the incoming flow direction, and the surface injection angle was 90 deg relative to the endwall. It did not open into the upstream slot and was fed by its own plenum to allow for independent control of the upstream slot and midpassage gap leakage flowrates. Figure 2(*c*) shows a section view of the midpassage gap with a simulated seal strip installed in the gap plenum. Inconel strips were attached to the inner channel walls of the midpassage gap, but only on the portion of the gap closest to the endwall surface. This portion of the gap was the foam material that comprised the flat endwall, whereas the other portions of the gap were made of polycarbonate with higher thermal conductivity. The Inconel strips were connected to a power supply by copper bus bars soldered to the Inconel in the same manner as for the upstream slot.

Coolant for the realistic leakage interfaces was extracted from the top bypass flow channel of the tunnel by a blower and sent to independent plenums for the upstream slot and midpassage gap. Flowrates to each plenum were controlled by valves. Coolant temperatures for both leakage flows were kept within 0.6°C of the mainstream flow temperature, resulting in a coolant-to-mainstream density ratio of 1.0. Leakage flowrates are given as a percent of the mass flow entering a vane passage. See Table 3 for the leakage flowrates and corresponding average blowing ratios and momentum flux ratios for each of the leakage interfaces.

Similar to the method of Cardwell et al. [11,12] and Lynch and Thole [2], the average leakage flowrate from the upstream slot was determined by multiplying the inviscid blowing ratio by an assumed discharge coefficient of 0.6 (based on the commonly accepted value for flow through a sharp-edged orifice [16]). For the midpassage gap, the leakage flowrate was directly measured with a laminar flow element placed in the gap coolant line. As described by Cardwell et al. [12], this method was necessary to determine net flowrate due to ingestion into the midpassage gap. The gap was maintained in the endwall (not covered) in all of the cases described in this paper, regardless of net leakage flowrate. For cases with no net leakage flow, the valve in the gap plenum supply line was closed.

3.2 Heat Transfer Measurements. Heat transfer coefficients were obtained on the endwall of the vane test section through infrared (IR) imaging of the surface temperatures on a uniform heat flux surface. See Kang et al. [14] for a detailed description of the heat transfer measurement procedure. The heat flux surface (total thickness of 0.25 mm) was made of Kapton-encapsulated Inconel foil in a serpentine pattern designed around the vanes and midpassage gap. A thin (37 μm) layer of copper was adhered to the top surface of the heater to distribute the heat flux uniformly. Flat black paint was sprayed thinly over the copper to increase surface emissivity for infrared measurements. The heater was attached to the 2.54 cm thick foam endwall described earlier, and E-type thermocouples for infrared image calibration were placed in thermal contact with the underside of the heater. Since the IR camera imaged the top surface of the heater, a one-dimensional correction for conduction bias due to thermal resistance of the heater was applied to the readings obtained from the underside-mounted thermocouples.

Surface temperatures on the heater were captured at steady-state conditions by directly imaging the bottom endwall from ports in the top endwall of the test section. The infrared camera had a resolution of 240×320 pixels, resulting in a resolution of 1.4 mm/pixel on the endwall. Five images were taken at each port and averaged to produce a measurement at that port. Apparent reflected temperature and surface emissivity were adjusted for each image so that the temperatures at the locations of the calibration thermocouples in the image matched the steady-state readings of those thermocouples. Typical values for emissivity and apparent reflected temperature were $\varepsilon=0.94$ and $T_{\mathrm{reflc}}=20°\mathrm{C}$, which agreed well with published emissivity for flat black paint ($\varepsilon=0.96$) and the measured freestream temperature ($T_\infty=23°\mathrm{C}$).

Heat transfer coefficients in the midpassage gap were obtained by measuring the surface temperature of the Inconel foil heater on the inner channel walls. Thermocouples were embedded in the foam underneath each heater in a nonuniformly spaced pattern along the length of the gap. Each thermocouple was placed in thermal contact with the underside of the heater. At steady-state conditions, approximately 600 samples were obtained at a sampling rate of 0.5 Hz and averaged to produce a measurement of the Inconel foil temperature at the location of the thermocouple. Heat transfer coefficients were nondimensionalized as a Nusselt number based on the hydraulic diameter of the gap.

Applied heat flux was the same for all heated surfaces in this study. For both the endwall heaters and the Inconel strip heaters on the upstream slot and midpassage gap surfaces, current supplied to the heaters was determined by measuring the voltage drop across a precision resistor (1 Ω) in series with the heater. The voltage drop across each heater was also measured to calculate total power delivered to each heater. The applied heat flux of 1300 $\mathrm{W/m^2}$ was determined by dividing the total power supplied

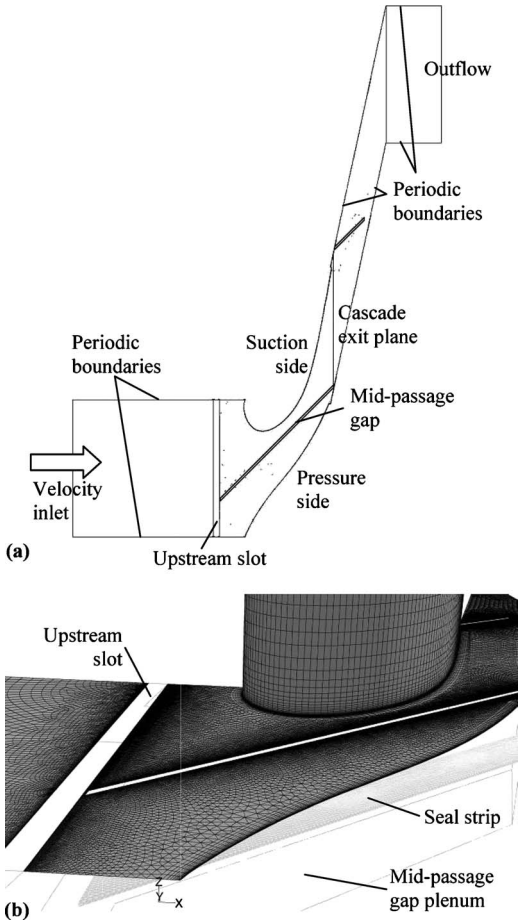

Fig. 3 (*a*) The computational domain with boundaries and (*b*) view of the endwall and suction-side airfoil mesh

to a heater by its area. Convective heat flux was calculated by subtracting conductive losses (<3%) through the bottom endwall and radiative losses to the surroundings (<17%, assuming black body radiation exchange with isothermal surroundings). Conduction and radiation corrections were applied locally, with the highest corrections occurring at the highest surface temperatures.

The partial derivative method of Moffat [17] was used to estimate experimental uncertainty of measured variables. Uncertainty in St number was dominated by uncertainty in the measured wall temperature. For that measurement, the bias uncertainty was estimated as $\pm 0.65\,^{\circ}\mathrm{C}$ by accounting for thermocouple bias and IR image bias. The precision uncertainty of $\pm 0.20\,^{\circ}\mathrm{C}$ was estimated by taking the standard deviation of six IR measurement sets, consisting of five images each. From these uncertainties, the overall uncertainty of the wall temperature was $\partial T_w = \pm 0.68\,^{\circ}\mathrm{C}$. Uncertainty in Stanton number was estimated as $\partial \mathrm{St} = \pm 0.0011$ (8.1%) at a high value of St=0.013, and $\partial \mathrm{St} = \pm 0.00013$ (3.3%) at a low value of St=0.004.

4 Computational Methodology

Predictions of the vane passage flowfield with an upstream slot and midpassage gap were performed using the commercially available computational fluid dynamics (CFD) software FLUENT [18]. All simulations used a pressure-based formulation for incompressible flow. The steady Reynolds-averaged Navier–Stokes (RANS) equations for momentum and energy were solved in double-precision using second-order finite-volume discretization with an upwinding scheme.

FLUENT's grid generation software GAMBIT was used to generate the unstructured mesh. Figure 3(*a*) indicates the domain for the computational study, while Fig. 3(*b*) shows the endwall and suction-side airfoil grid. A single passage of the vane cascade was modeled with periodic boundaries in the pitchwise direction, whereby the periodic boundaries passed through the vane stagnation and vane trailing edge. The vane was modeled from the endwall to the midspan, and a symmetry condition was implemented at the midspan boundary. A constant heat flux boundary condition was specified on the endwall and leakage interface surfaces in the same manner as the experimental setup. A velocity inlet was located $1.2C$ upstream of the vane stagnation. At the inlet, a 1/7 power law velocity profile corresponding to the measured boundary layer thickness was implemented for the streamwise velocity component. The inlet turbulence level and length scale were set to 1% and 0.0594 m ($0.10C$), respectively. The grid extended $1.75C$ downstream of the vane trailing edge, followed by a rectangular section extending $0.3C$ in the X-direction to reduce skewed cells at the exit plane. The exit was set to an outflow boundary condition. The upstream slot and midpassage gap plenums in the computational study were replicated from the experimental geometry, and mass-flow inlets were specified for each plenum.

The boundary layer mesh capability in GAMBIT was used to generate a grid with a wall spacing of approximately $y^+=1$ on the vane, endwall, upstream slot, and midpassage gap surfaces. This was necessary for the k-ω shear stress transport (SST) turbulence model used in this study. FLUENT's adaptive grid refinement tools were used to ensure y^+ values less than 1 on the surfaces of interest as the solution converged.

Two turbulence models (k-ω SST and renormalization group (RNG) k-ε) available in FLUENT were compared in this study. The k-ω SST model is a low-Reynolds number model that blends the standard k-ω model appropriate near the wall, with a modified k-ε model in the freestream. According to FLUENT [18] documentation, this makes the k-ω SST model particularly appropriate for flows with adverse pressure gradients and airfoils. The RNG k-ε model with nonequilibrium wall functions was shown by Hermanson and Thole [19] to exhibit good agreement between measurements and predictions of secondary flow for the same vane as in this study. The near-wall resolution ($y^+ \approx 1$) of the grid in this study required the use of the enhanced wall treatment option for the RNG k-ε model, instead of wall functions.

Two conditions were tested to determine solution convergence: normalized residual levels and surface averages. Iterations were performed until normalized residuals did not change, which corresponded to levels below 10^{-4} for continuity, momentum, and turbulence quantities (k, ω, ε) and 10^{-6} for energy. Area-averaged St values on the endwall, and mass-averaged total pressure loss on a plane at $1.02C_{ax}$ downstream of the vane, were also monitored during the calculations. The solution was considered fully converged when those values changed by less than 1% over 400 iterations after achieving convergence with normalized residuals. Convergence was generally achieved within 1500 iterations.

Grid independence was tested by comparing successive grid refinements. The original grid contained approximately 7.7×10^6 cells. A refinement based on y^+ values increased the grid size to 8.1×10^6 cells. Area-averaged St for the refined grid was decreased by 10%, and mass-averaged C_{Ptot} was decreased by 1.1%. A second refinement increased the grid to 9.6×10^6 cells, with a subsequent decrease of 1.1% in area-averaged St and 0.06% in mass-averaged C_{Ptot} relative to the previous refinement. A third refinement resulted in a grid with 11.3×10^6 cells, and further reductions of 0.7% and 0.3% in area-averaged St and mass-averaged C_{Ptot}, respectively. The largest grid (11.3×10^6 cells) was used for the results presented in this paper.

5 Results and Discussion

Several studies were performed to determine the effect of the upstream slot and midpassage gap on endwall heat transfer. First, the effect of the upstream slot location relative to the vane leading

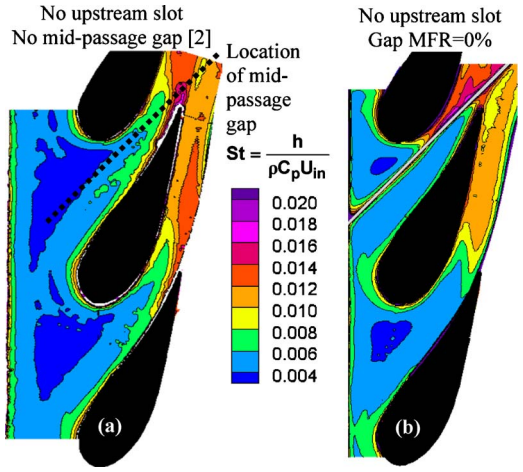

Fig. 4 Comparison of endwall heat transfer with no upstream slot for (*a*) no gap [2] and (*b*) this study with 0% MFR from the midpassage gap

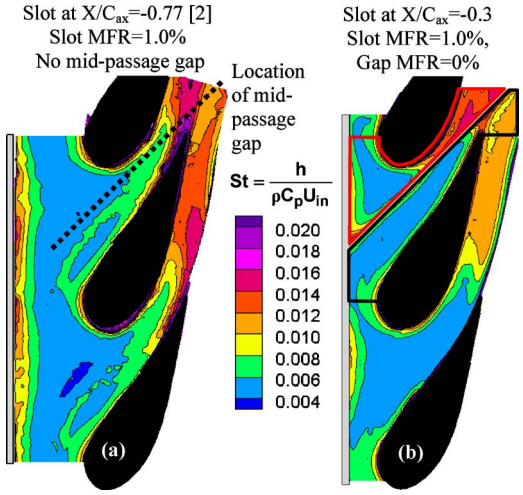

Fig. 5 Endwall heat transfer with an upstream slot blowing at 1.0% MFR for a slot at (*a*) $X/C_{ax}=-0.77$ [2] versus at (*b*) $X/C_{ax}=-0.3$

edge is discussed, followed by the effect of the midpassage gap relative to a smooth endwall. Predictions of the endwall heat transfer with an upstream slot and midpassage gap are presented next. Measured heat transfer contours are shown for various leakage flowrates from the upstream slot and midpassage gap. Finally, endwall heat transfer is compared with the adiabatic film-cooling measurements of Cardwell et al. [12].

5.1 Measured Effects of Leakage Interfaces. A contour map of measured endwall heat transfer without an upstream slot is compared with the results of Lynch and Thole [2] with no upstream slot in Fig. 4. In both cases, there is an unheated starting length effect, seen as a thin region of high heat transfer gradients at the leading edge of the heater, since the velocity boundary layer began farther upstream. It is important to note that the heater in the study of Lynch and Thole [2] extended $0.77C_{ax}$ upstream of the vane stagnation compared with $0.3C_{ax}$ in this study. This difference in unheated starting length explains the smaller size of the region of low St values between the lower and middle vanes in Fig. 4(*b*) compared with Fig. 4(*a*). Strong endwall secondary flows in the passage generally tend to wash out differences between unheated starting lengths elsewhere when comparing the vane passage without a midpassage gap (lower part of Fig. 4(*b*)) to the results of Lynch and Thole [2] in Fig. 4(*a*).

Figure 5 compares endwall St contours with 1.0% mass-flow ratio (MFR) from an upstream slot located at $X/C_{ax}=-0.77$ (Fig. 5(*a*), from Lynch and Thole [2]) versus an upstream slot at $X/C_{ax}=-0.3$ also at 1.0% MFR (Fig. 5(*b*)). Relative to the contours in Fig. 4, Fig. 5 indicates that an upstream slot with blowing generally increases heat transfer immediately downstream of the slot. The addition of leakage flow to the incoming boundary layer increases the near-wall velocity and thus increases heat transfer downstream of the slot. The region of high heat transfer downstream of the slot, however, is much more uniform in the pitchwise direction for the slot located far upstream of the vane (Fig. 5(*a*)) versus a slot located closer to the vane (Fig. 5(*b*)). This is because the pressure field imposed by the vanes forces leakage flow from the upstream slot in Fig. 5(*b*) to exit in a nonuniform manner. This effect is illustrated in Fig. 6, where nondimensionalized slot leakage velocity is plotted along the pitchwise direction. The pitchwise coordinate is based on the vane coordinate system, such that $Y/P=0$ corresponds to the stagnation point on the center vane. Slot velocities in Fig. 6 were determined by calculating the local inviscid velocity of the leakage flow at a pitchwise location using the pressure difference between the slot plenum and the local endwall static pressure, and then multiplying by the assumed discharge coefficient described earlier. Figure 6 indicates that for the slot located at $X/C_{ax}=-0.77$, the slot leakage velocity at 1.0% MFR is positive and fairly uniform over the entire pitch of the cascade. In contrast, the slot leakage velocity at 1.0% MFR for the slot at $X/C_{ax}=-0.3$ exhibits a large variation in amplitude, with negative velocities (ingestion) upstream of the vane stagnation.

The effect of a closed midpassage gap (no net blowing) with no upstream slot can be determined by comparing the upper passages of Figs. 4(*a*) and 4(*b*). Note that in an engine, both the upstream slot and midpassage gap would be present; however, the case presented in Fig. 4(*b*) isolates the effect of the gap on endwall heat transfer. In general, the midpassage gap tends to significantly increase St values in the latter part of the passage. In Fig. 4(*b*), the upper passage with the gap shows a high gradient in St on the suction-side platform at the leading edge of the gap (near the upstream slot). This is due to flow being ingested into the gap; Cardwell et al. [11] showed that gap ingestion velocity was highest at the gap leading edge. The region where the gap passes close to the suction side of the upper vane in Fig. 4(*b*) also has high heat transfer levels relative to a continuous passage (Fig. 4(*a*)). Downstream of that point, a spike of high St values is seen near the throat in Fig. 4(*b*). Note that the high levels of heat transfer are

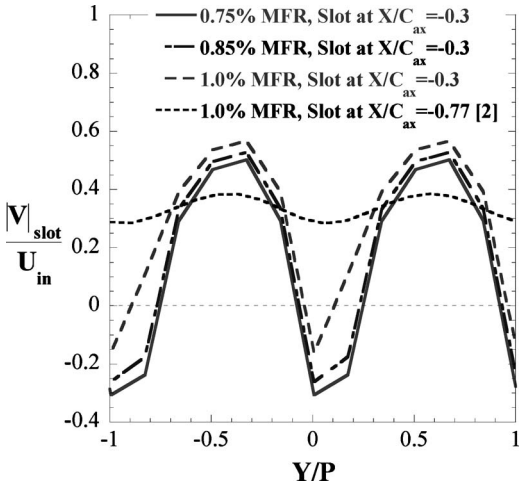

Fig. 6 Nondimensional leakage velocity from the upstream slot for varying slot flowrates and locations upstream of the vane

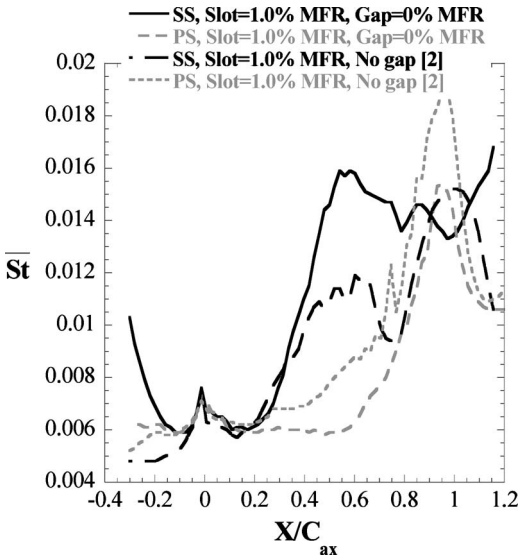

Fig. 7 A comparison of pitchwise-averaged heat transfer for the suction side and pressure side of the endwall around the midpassage gap

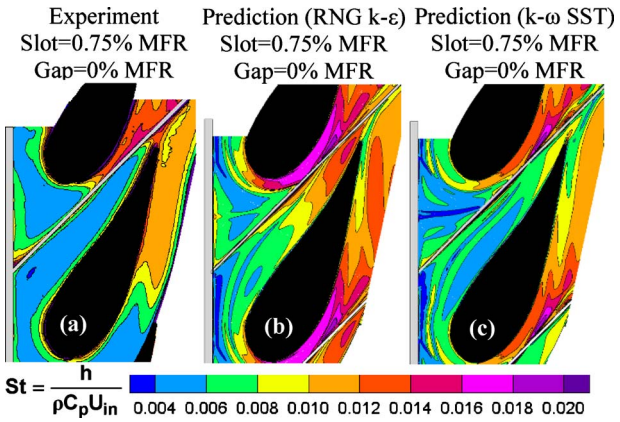

Fig. 8 Endwall heat transfer for 0.75% slot MFR and 0% gap MFR from (*a*) experimental results and from predictions using the (*b*) RNG *k-ε* and (*c*) *k-ω* SST turbulence models in FLUENT [18]

mainly on the suction-side platform (the endwall region associated with the uppermost vane). Some increased heat transfer around the gap, relative to a passage without a gap, is also seen on the pressure-side platform.

The combined effect of an upstream slot with blowing and a closed midpassage gap (0% MFR) can be seen by comparing the upper passages of Figs. 4(*b*) and 5(*b*). As noted earlier, upstream slot blowing tends to increase heat transfer downstream of the slot. Also, the high St values near the gap leading edge are further increased with upstream slot blowing. Further into the passage, there are relatively few differences between Figs. 4(*b*) and 5(*b*), indicating little effect of the upstream slot flow.

Figure 7 shows pitchwise-averaged values of heat transfer plotted versus normalized axial coordinate (X) through the cascade for the PS and SS platforms of the upper passages in Figs. 5(*a*) and 5(*b*). The averaging regions for the pressure-side and suction-side platforms are outlined in Fig. 5(*b*). Pitchwise-averaged St values were computed in those regions for both cases in Fig. 5. Comparisons of pitchwise-averaged St between the suction- and pressure-side platforms in Fig. 7 for an endwall with a midpassage gap (Fig. 5(*b*)) show that heat transfer levels are generally higher on the suction-side platform. Considering the same pitchwise-averaging regions for an endwall without a midpassage gap (Lynch and Thole [2]), it is apparent that the discrepancy between the suction-side and pressure-side platform heat transfers, particularly between $0.2 < X/C_{ax} < 0.7$, is not as large as for an endwall with a gap. Furthermore, the suction-side platform heat transfer for a continuous endwall is generally lower than for an endwall with a gap, downstream of $X/C_{ax}=0.4$. This is an important point since preliminary turbine designs may be based on endwall heat transfer predictions for an endwall without a gap. For this vane, at a location around $X/C_{ax}=0.5$, Fig. 7 indicates that the suction-side platform heat transfer with a gap could be higher than the heat transfer for an endwall with no gap. Note that the form of the endwall heat transfer pattern and the effect of a midpassage gap would be dependent on the airfoil geometry.

5.2 Predicted Effects of Leakage Interfaces. A computational study of the baseline leakage condition (0.75% slot MFR and 0% gap MFR) was performed to gain additional insight into the effect of the leakage interfaces. Figure 8 shows measured and predicted endwall heat transfers for the baseline leakage condition. The RNG *k-ε* model in Fig. 8(*b*) appears to do a better job of predicting the heat transfer downstream of the upstream slot, but significantly overpredicts endwall heat transfer further into the passage near the pressure side of the vane. Conversely, the *k-ω* SST model (Fig. 8(*c*)) underpredicts the heat transfer downstream of the slot, but appears to do a better job matching the experimental results (Fig. 8(*a*)) near the vane pressure side. On the suction-side platform near the throat, the *k-ω* SST model shows good qualitative and quantitative agreements with the measurements. At this location, the RNG *k-ε* model also indicates good qualitative agreement with the measured endwall heat transfer pattern, although St values are overpredicted near the vane endwall junction. This agreement between measured and predicted heat transfers is especially significant since that region has such high St relative to an endwall without a gap, as was described earlier.

Figure 9 is a plot of endwall heat transfer with streamlines from

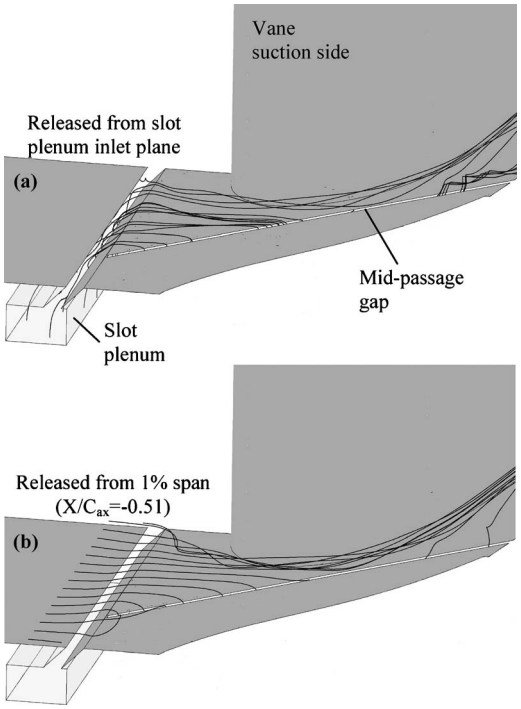

Fig. 9 Streamlines released from (*a*) the upstream slot plenum inlet and (*b*) from 1% span at $X/C_{ax}=-0.51$ upstream of the vane

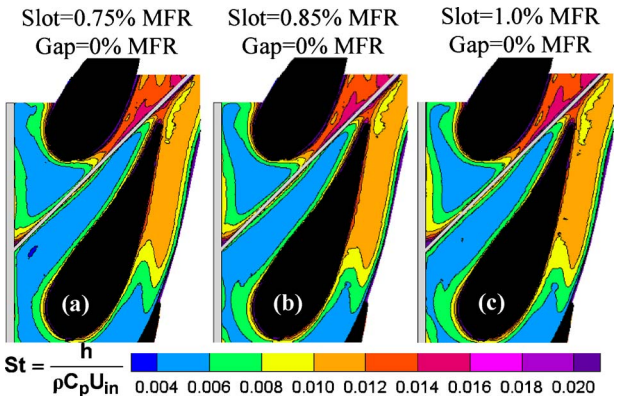

Fig. 10 Endwall heat transfer for 0% MFR from the midpassage gap and upstream slot flowrates of (*a*) 0.75% MFR, (*b*) 0.85% MFR, and (*c*) 1.0% MFR

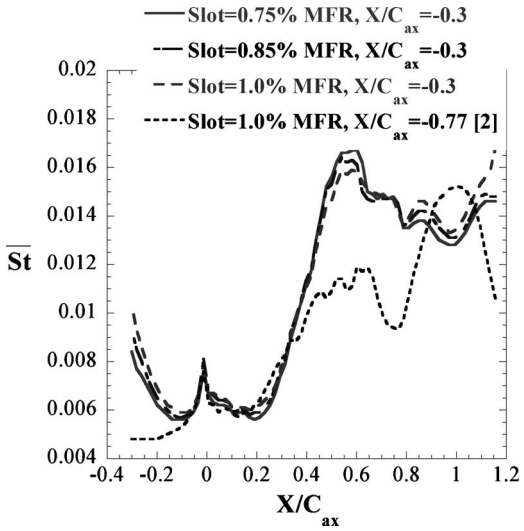

Fig. 11 Pitchwise-averaged endwall St values on the suction-side platform for 0% MFR from the midpassage gap and varying upstream slot flowrates

the k-ω SST model prediction. Streamlines were released at the inlet to the slot plenum in Fig. 9(*a*). In Fig. 9(*b*), streamlines were released upstream of the vane at $X/C_{ax}=-0.51$, from a line located at 1% of the span from the endwall. The streamlines indicate the large amount of ingestion of near-wall and upstream slot flow into the gap. That fluid is convected through the gap and ejected near the low-pressure region at the throat. The ejected fluid appears to roll up into a small vortex, where the downwash of that vortex corresponds to the peak of high endwall heat transfer seen in the measurements and computations.

5.3 Measured Effect of Upstream Slot Leakage Flow. The effect of upstream slot leakage flowrate for the endwall with a midpassage gap is illustrated by the St contours in Fig. 10. As described earlier, increasing the upstream slot flowrate generally increases the heat transfer immediately downstream of the slot. Figure 6 shows the slot leakage velocity increasing with slot MFR, whereby higher slot leakage velocities result in higher heat transfer rates on the endwall downstream of the slot.

Downstream of the slot in Fig. 10, the dominating effect of endwall secondary flows results in similar St contours in the passage for Fig. 10. There is, however, a slight increase in the size of the peak of high heat transfer on the suction-side platform at the vane throat, as slot MFR is increased. Increased slot blowing provides more low-momentum fluid to be ingested into the gap, resulting in turbulent mixing and higher rates of endwall heat transfer where the flow is ejected. Pitchwise-averaged heat transfer in Fig. 11 indicates slightly higher heat transfer immediately downstream of the slot and downstream of $X/C_{ax}=0.75$ for increasing slot leakage flow. Between those points, the dominant effect of the endwall secondary flows results in pitchwise-averaged values of St which are fairly similar over the range of upstream slot leakage.

5.4 Measured Effect of Midpassage Gap Flow. Figure 12 shows endwall heat transfer with increasing net leakage flow from the midpassage gap. Cardwell et al. [12] indicated that the ingestion-ejection mechanism of the gap, and its effect on the endwall adiabatic effectiveness and gap temperature, was insensitive to gap net flowrates of up to 0.3% MFR. Based on the results in Fig. 12, the same can be said for the endwall heat transfer; namely, that net gap leakage flowrates as high as 0.5% MFR do not appear to have a significant effect, except to slightly increase the size of the peak of high heat transfer at the gap ejection location in the vane throat. Pitchwise-averaged results for the suction-side vane platform in Fig. 13 indicate a slight increase in heat transfer from $0.65<X/C_{ax}<1.2$ with increasing gap flowrates. Leakage flow introduced to the gap plenum is more likely to exit the gap in the region of low static pressure in the vane throat, contributing to high levels of endwall heat transfer.

Heat transfer measurements on the pressure-side and suction-side inner walls of the midpassage gap are shown in Fig. 14. In general, for both sides of the gap Nu values gradually increase from $x_g/L=0$ to approximately $x_g/L=0.25$, where the streamlines in Fig. 9 indicate that low-momentum turbulent upstream slot leakage flow is being ingested into the gap. Beyond $x_g/L=0.25$, heat transfer gradually decreases as the gap ingestion velocity becomes lower until Nu values reach a minimum at $x_g/L=0.50$. This is the same location that Cardwell et al. [11] showed to have zero ejection velocity based on an inviscid calculation. Further along the gap, as the gap ejection velocity increases, the gap heat transfer also increases.

Nusselt values for the gap pressure-side wall versus the suction-side wall do not appear to be dramatically different in Fig. 14. Slightly higher values of Nu are seen on the pressure side relative to the suction side between $0.25<x_g/L<0.5$ due to the ingested flow impinging preferentially on that side of the gap. A peak is seen in the suction-side Nu values at $x_g/L<0.65$, which corresponds to the peak endwall St value in the throat region described earlier.

Only a slight increase in gap wall Nu values is seen with increasing gap MFR, which is consistent with the endwall St results in Fig. 12. Note from Fig. 14 that the pressure-side heat transfer at a gap MFR of 0.5% shows slightly lower Nu from $0.2<x_g/L<0.5$, and slightly higher Nu from $0.6<x_g/L<0.9$, relative to the

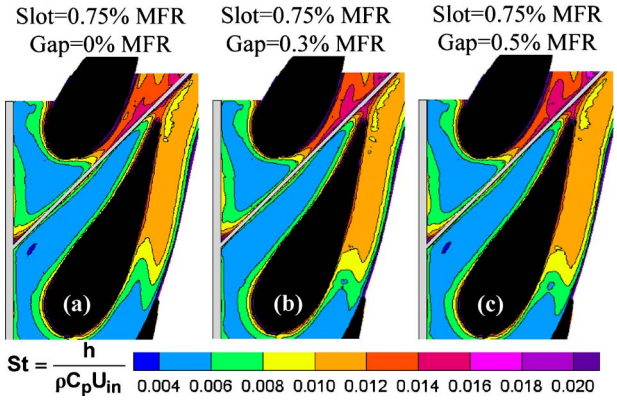

Fig. 12 Endwall heat transfer for 0.75% MFR from the upstream slot and midpassage gap flowrates of (*a*) 0% MFR, (*b*) 0.3% MFR, and (*c*) 0.5% MFR

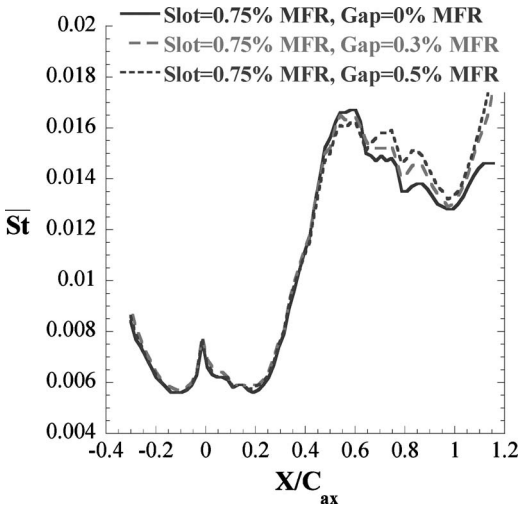

Fig. 13 Pitchwise-averaged endwall heat transfer on the suction-side platform for varying midpassage gap flowrates

other gap flowrates. Although the effect is small, 0.5% MFR might prevent some ingestion into the upstream part of the gap. However, a large part of the mass flow will also be ejected in the downstream part of the gap and will enhance heat transfer there.

5.5 Comparison to Measured Adiabatic Effectiveness. Contours of endwall heat transfer at two upstream slot flowrates are compared with contours of adiabatic film effectiveness at corresponding slot MFR (Cardwell et al. [12]) in Fig. 15. Fortunately, high St values downstream of the slot for 0.75% MFR (Fig. 15(*a*)) are in a region of high adiabatic film effectiveness (Fig. 15(*c*)), so this region would likely remain cool. As the upstream slot flowrate is increased, Fig. 15(*b*) indicates that heat transfer increases, but Fig. 15(*d*) also indicates that cooling effectiveness increases.

Other regions of the endwall are more likely to see high heat flux due to low film effectiveness levels and high heat transfer. In particular, the discrete holes at the vane endwall junction near the vane stagnation in Figs. 15(*c*) and 15(*d*) appear to be providing some cooling to that region, but the corresponding heat transfer levels (Figs. 13(*a*) and 13(*b*)) are high at the vane endwall junction. Even more critical is the throat region, where the gap ejects flow. The streak of low effectiveness seen in Figs. 15(*c*) and 15(*d*) near the throat appears to be located close to the spike of high St values in Figs. 15(*a*) and 15(*b*), which is a very undesirable situation for turbine durability. Increasing the upstream slot MFR from 0.75% to 1.0% slightly exacerbates the heat transfer coefficients in this region (compare Fig. 15(*a*) to Fig. 15(*b*)), and adiabatic effectiveness contours appear to be unchanged (compare Figs. 15(*c*) and 15(*d*)), so this would not be a viable option to reduce heat flux experienced by the part.

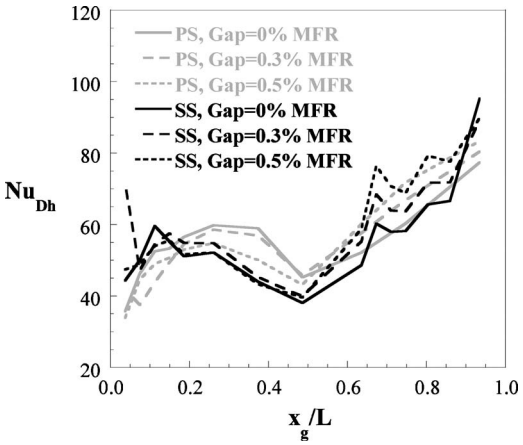

Fig. 14 Heat transfer on the inner channel walls of the midpassage gap for 0.75% upstream slot MFR and varying midpassage gap flowrates

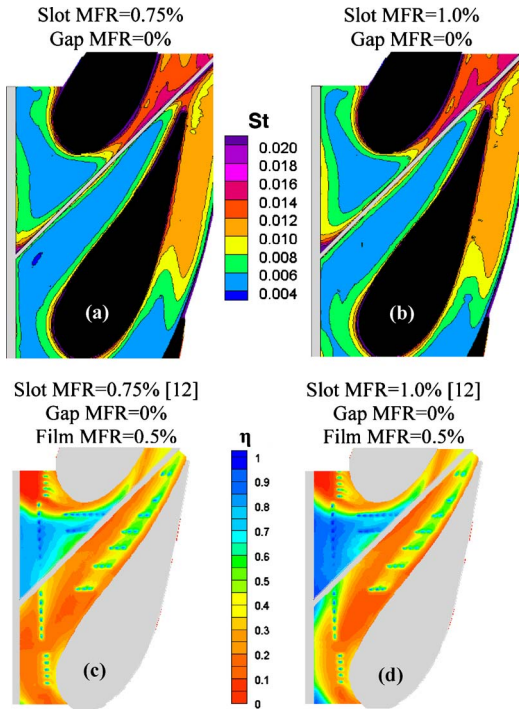

Fig. 15 Comparison of endwall heat transfer for slot MFRs of (*a*) 0.75% and (*b*) 1.0% to adiabatic film effectiveness [12] at slot MFRs of (*c*) 0.75% and (*d*) 1.0%

Cardwell et al. [12] showed that increasing the gap leakage from 0% to 0.3% MFR did not increase endwall adiabatic film effectiveness, so increasing the gap leakage flow would also not appear to provide any reduction in heat flux. However, Hada and Thole [13] indicated that decreasing the seal strip clearance (increasing the plenum supply pressure) increased gap leakage cooling effectiveness and uniformity since less flow was ingested into the gap. Unfortunately, the seal strip clearance is difficult to control in an engine. Another option to reduce heat flux near the throat could be to add discrete film holes; however, the ejected flow from the gap may facilitate jet separation.

6 Conclusions

Experimental measurements of endwall heat transfer were presented for an endwall with an upstream slot and a midpassage gap. These features were designed to simulate realistic leakage interfaces that are present between individual components in a gas turbine engine. In addition to the measurements, a computational study was performed for the baseline leakage condition.

The location of the upstream slot relative to the leading edge of the vane was seen to influence heat transfer levels downstream of the slot. For a slot located at $X/C_{ax}=-0.3$, St values were higher between vanes than in front of the vane stagnation. This effect was linked to the variation in upstream slot leakage velocity caused by the pressure field around the vane.

Heat transfer coefficients around the vane passage throat were significantly higher for the endwall with a midpassage gap than for an endwall without a gap. Near-wall flow is ingested into the gap upstream and ejected at the vane passage throat, causing high levels of heat transfer there. Streamlines from the computational study indicated that a small separation vortex was created where

flow was ejected from the gap at the vane passage throat. This vortex sweeps fluid down onto the endwall, causing increased heat transfer.

Increasing amounts of leakage flow from the upstream slot increased heat transfer immediately downstream of the slot, but had a very slight effect elsewhere in the vane passage. Midpassage gap leakage flowrates of up to 0.5% of the passage mass flow had little effect on the endwall heat transfer. Heat transfer coefficients on the inner channel walls of the midpassage gap were higher at the downstream portion of the gap due to high ejection velocity and were also relatively insensitive to gap leakage flowrate.

Heat transfer contours at two upstream slot flowrates were compared with adiabatic film effectiveness measurements of Cardwell et al. [12] for the same endwall leakage interface configuration. Upstream slot leakage flow resulted in high heat transfer levels but also high effectiveness levels, suggesting that the part would remain relatively cool in that region. In comparison, the high heat transfer in the vane passage throat region was located in a region with low cooling effectiveness, indicating that the part would be likely to experience high metal temperatures and large thermal stresses at that location.

Acknowledgment

The authors would like to acknowledge Narayan (Sundar) Sundaram and J. Ryan McHale for their help in the design and construction of the test section.

Nomenclature

A_c = cross-sectional area of flow through slot or gap
BL = boundary layer
C = true chord of vane
C_{ax} = axial chord of vane
C_p = specific heat at constant pressure or static pressure coefficient $C_p=(P_s-P_{s,in})/0.5\rho U_{in}^2$
D_h = hydraulic diameter, $D_h=4A_c/P$
h = heat transfer coefficient, $h=q''_w/(T_w-T_{in})$
I = average momentum flux ratio, $I=M^2(\rho_{in}/\rho_j)$
k = thermal conductivity or turbulent kinetic energy
L = gap length
M = average blowing ratio, $M=(\dot{m}_j/A_{c,j})/(\dot{m}_{in}/A_{c,in})$
MFR = mass-flow ratio, MFR$=\dot{m}_j/\dot{m}_{in}$
Nu_{D_h} = Nusselt number, Nu$=hD_h/k_{air}$
P = vane pitch or perimeter of the gap flow area
P_s = static pressure
PS = pressure side
q''_w = wall heat flux
Re_{in} = inlet Reynolds number, $Re_{in}=CU_{in}/\nu$
Re_θ = momentum thickness Re number, $Re_\theta=\theta U_{in}/\nu$
RNG = renormalization group
S = vane span
SS = suction side
SST = shear stress transport
St = Stanton number, St$=h/\rho C_p U_{in}$
$\overline{\text{St}}$ = pitchwise-averaged Stanton number
T = temperature
T_{reflc} = average temperature associated with radiation reflected off the endwall from the surroundings
x_g = midpassage gap lengthwise coordinate
X, Y, Z = global coordinates, where X is the vane axial direction
U, V, W = axial, pitchwise, and spanwise velocities
$|V|$ = velocity magnitude

Greek

δ = boundary layer thickness
ε = emissivity or dissipation
θ = momentum thickness
ν = kinematic viscosity
ρ = density
ω = specific dissipation

Subscripts/Superscripts

exit = exit freestream conditions
in = inlet freestream conditions
j = coolant conditions
slot = upstream slot conditions
w = wall conditions

References

[1] Knost, D. G., and Thole, K. A., 2003, "Computational Predictions of Endwall Film-Cooling for a First-Stage Vane," ASME Paper No. GT2003-38252.
[2] Lynch, S. P., and Thole, K. A., 2008, "The Effect of Combustor-Turbine Interface Gap Leakage on the Endwall Heat Transfer for a Nozzle Guide Vane," ASME J. Turbomach., **130**, p. 041019.
[3] Rehder, H.-J., and Dannhauer, A., 2007, "Experimental Investigation of Turbine Leakage Flows on the Three-Dimensional Flow Field and Endwall Heat Transfer," ASME J. Turbomach., **129**, pp. 608–618.
[4] Aunapu, N. V., Volino, R. J., Flack, K. A., and Stoddard, R. M., 2000, "Secondary Flow Measurements in a Turbine Passage With Endwall Flow Modification," ASME J. Turbomach., **122**, pp. 651–658.
[5] Reid, K., Denton, J., Pullan, G., Curtis, E., and Longley, J., 2007, "The Interaction of Turbine Inter-Platform Leakage Flow With the Mainstream Flow," ASME J. Turbomach., **129**, pp. 303–310.
[6] Reid, K., Denton, J., Pullan, G., Curtis, E., and Longley, J., 2006, "Reducing the Performance Penalty Due to Turbine Inter-Platform Gaps," ASME Paper No. GT2006-90839.
[7] Piggush, J. D., and Simon, T. W., 2005, "Flow Measurements in a First-Stage Nozzle Cascade Having Endwall Contouring, Leakage and Assembly Features," ASME Paper No. GT2005-68340.
[8] Piggush, J. D., and Simon, T. W., 2005, "Heat Transfer Measurements in a First-Stage Nozzle Cascade Having Endwall Contouring, Leakage and Assembly Features," ASME Paper No. HT2005-72573.
[9] Piggush, J. D., and Simon, T. W., 2006, "Adiabatic Effectiveness Measurements in a First-Stage Nozzle Cascade Having Endwall Contouring, Leakage, and Assembly Features," ASME Paper No. GT2006-90576.
[10] Ranson, W. W., Thole, K. A., and Cunha, F. J., 2005, "Adiabatic Effectiveness Measurements and Predictions of Leakage Flows Along a Blade Endwall," ASME J. Turbomach., **127**, pp. 609–618.
[11] Cardwell, N. D., Sundaram, N., and Thole, K. A., 2006, "Effect of Midpassage Gap, Endwall Misalignment, and Roughness on Endwall Film-Cooling," ASME J. Turbomach., **128**, pp. 62–70.
[12] Cardwell, N. D., Sundaram, N., and Thole, K. A., 2007, "The Effects of Varying the Combustor-Turbine Gap," ASME J. Turbomach., **129**, pp. 756–764.
[13] Hada, S., and Thole, K. A., 2006, "Computational Study of a Midpassage Gap and Upstream Slot on Vane Endwall Film-Cooling," ASME Paper No. GT2006-91067.
[14] Kang, M. B., Kohli, A., and Thole, K. A., 1999, "Heat Transfer and Flowfield Measurements in the Leading Edge Region of a Stator Vane Endwall," ASME J. Turbomach., **121**, pp. 558–568.
[15] Radomsky, R. W., and Thole, K. A., 2000, "Flowfield Measurements for a Highly Turbulent Flow in a Stator Vane Passage," ASME J. Turbomach., **122**, pp. 255–262.
[16] Munson, B. R., Young, D. F., and Okiishi, T. H., 2002, *Fundamentals of Fluid Mechanics*, 4th ed., Wiley, New York, p. 514.
[17] Moffat, R. J., 1988, "Describing the Uncertainties in Experimental Results," Exp. Therm. Fluid Sci., **1**, pp. 3–17.
[18] FLUENT (version 6.3.26), Fluent Inc., Lebanon, NH.
[19] Hermanson, K., and Thole, K. A., 2000, "Effect of Inlet Profiles on Endwall Secondary Flows," J. Propul. Power, **16**, pp. 286–296.